

Electron Tunneling in Monolayer and Bilayer Graphene

Di Wu, Weiqiang Chen and Fu-Chun Zhang

*Department of Physics, and Center for Theoretical and Computational Physics,
The University of Hong Kong, Pokfulam Road, Hong Kong, China*

(Dated: February 10, 2022)

Electron's tunneling through potential barrier in monolayer and bilayer graphene lattices is investigated by using full tight-binding model. Emphasis is placed on the resonance tunneling feature and inter-valley scattering probability. It is shown that normal incidence transmission probabilities for monolayer and bilayer graphene exhibit different properties. Our calculation indicates that valleytronics in graphene systems may be detected, generated and controlled by changing the structure parameters of the external electric potential.

I. INTRODUCTION

Recently, great interest has been aroused in research on the physical properties of graphene, a one-atom-thick allotrope of carbon, due to its successful fabrication in 2004¹. Monolayer graphene is a truly two-dimensional material, with unusual electronic excitations described in terms of Dirac fermions that move in a curved space². The electrons in graphene seem to be almost insensitive to disorder and electron-electron interactions and have very long mean free path³. Hence, graphene's transport properties are rather different from what is found in usual metals and semiconductors. Interestingly enough, these properties can be easily modified with the application of electric and magnetic fields, the addition of layers, and by controlling its geometry and chemical doping⁴. Apart from the interesting fundamental physics in this new system, graphene is attracting attention as a promising new material for electronic applications. For a review concerning the history, fabrication, fundamental properties, and future applications of graphene, we refer to the recent article⁵.

The low energy charge carriers in graphene are described by a massless Dirac equation and have a linear energy dispersion which is isotropic near the Dirac points where the valence and conduction bands meet each other⁶. Such characteristics offer exciting opportunities for the occurrence of new tunneling phenomena and the development of high quality devices. Therefore, it may be valuable to investigate the electronic transport properties of graphene. In this regards, much of the phenomena associated with tunneling in graphene systems has been theoretically studied^{7,8,9,10,11}. It is interesting that, owing to the chiral nature of the quasiparticles, the propagation of charge carriers in monolayer graphene mimics the tunneling of massless fermions. This relativistic effect provides us an experiment test for the Klein paradox^{7,12}, which predicts that electron can pass through a high potential barrier to approach the perfect transmission. In contrast, for conventional non-relativistic particles, the transmission probability exponentially decays with the increasing of the barrier height. Besides this relativistic transport feature, other promising tunneling properties of graphene systems are the ability to tune the carrier density through a gate voltage¹, the absence of back scattering¹³, and the fact that graphene exhibits both spin and valley degrees of freedom¹⁴, which might be harnessed in envisaged spintronic^{15,16} or valleytronic devices¹⁷.

However, in these previous studies, considering the carriers as massless fermions remains an approximation, and we expect a deviation from a linear dispersion for high energies of the Dirac cone¹⁸. To this end, it is both important and interesting to study the transport properties in graphene system without this approximation. In this work, we investigate the tunneling properties of both monolayer and bilayer graphene lattice by using the full tight-binding model. This paper is organized as follows. In Sec. II, we introduce the model of the system that we are considering and give explicit expressions for the wave functions in different regions through tunneling process. We also provide some details on how to compute the transmission amplitudes. In Sec. III, we present the results for transmission probabilities in different barrier setups and the discussions. A brief summary and conclusion of the paper can be found in Sec. IV.

II. MODEL

We consider two kinds of lattice structure, each consisting respectively of monolayer graphene or bilayer graphene. A schematic picture of the system is shown in Fig. 1. The basic structure involves a graphene sheet and a one dimensional trapezoid shape potential $V(\mathbf{r}) = V(x)$, which is y -independent. In the following we will introduce the tight-binding model of graphene with this external electric potential.

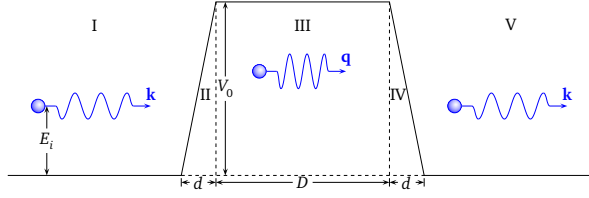


FIG. 1: Schematic of the external potential profile in graphene lattice. The energy of incident electron is E_i and the potential height is V_0 . There are five different regions in this tunneling process which are marked by roman numbers.

A. Tunneling in monolayer graphene lattice

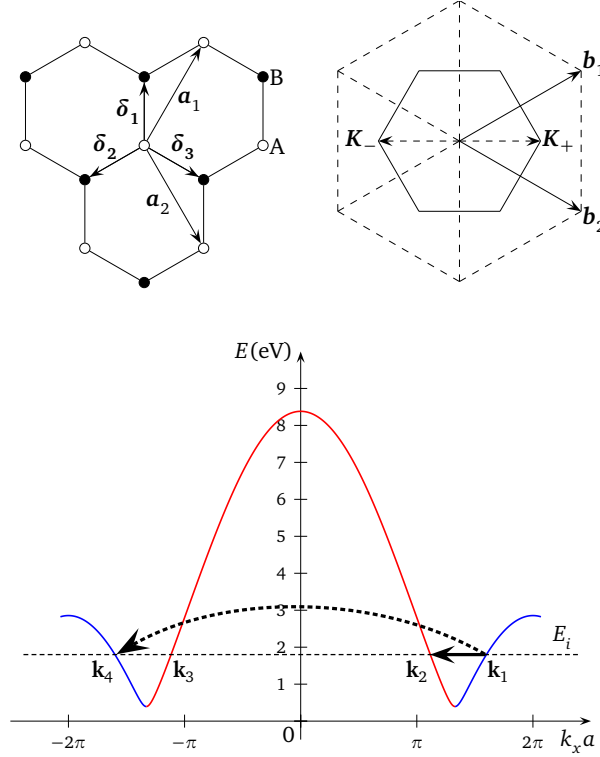


FIG. 2: Schematics of the lattice structure and the energy spectrum of monolayer graphene. Top left: Lattice structure of monolayer graphene, made out of two interpenetrating triangular lattice (\mathbf{a}_1 and \mathbf{a}_2 are the lattice unit vectors, and δ_i , $i = 1, 2, 3$ are the nearest neighbor vectors). Top right: The solid hexagon is a Brillouin zone. Dirac cones sit at the \mathbf{K}_+ and \mathbf{K}_- points. The reciprocal lattice vectors are \mathbf{b}_1 and \mathbf{b}_2 . Bottom: The energy spectrum of electrons at a finite k_y . There are four degenerate states for a given k_y when incident energy E_i is small. Two of these states (\mathbf{k}_1 and \mathbf{k}_4) have pseudo-spin $+1$, the other two states (\mathbf{k}_2 and \mathbf{k}_3) have pseudo-spin -1 . The solid arrow is the intra-valley scattering process (flip pseudo-spin) while the dashed arrow is the inter-valley scattering process (does not flip pseudo-spin).

The honeycomb lattice of monolayer graphene can be described in terms of two triangular sublattices, A and B (see Fig. 2). A unit cell contains two atoms, one of type A and one of type B. The lattice vectors can be written as $\mathbf{a}_1 = a(1/2, \sqrt{3}/2)$, $\mathbf{a}_2 = a(-1/2, \sqrt{3}/2)$, where $a \approx 2.46\text{\AA}$ is the lattice constant¹⁹. The reciprocal lattice vectors are given by $\mathbf{b}_1 = \frac{2\pi}{a}(1, 1/\sqrt{3})$ and $\mathbf{b}_2 = \frac{2\pi}{a}(1, -1/\sqrt{3})$.

In monolayer graphene, an atom of type A is connected to its nearest neighbors on B sites by three vectors δ_i . The nearest hopping tight-binding Hamiltonian describing this system has the form⁵

$$H_0 = -t \sum_{\langle i,j \rangle, \sigma} \left(a_{\sigma,i}^\dagger b_{\sigma,j} + \text{h.c.} \right), \quad (1)$$

where $t(\approx 2.8\text{eV})$ is the nearest neighbor hopping energy, $a_{\sigma,i}$ and $b_{\sigma,j}$ are the annihilation operators of electrons with spin $\sigma(\sigma = \uparrow, \downarrow)$ on A and B sublattices, respectively. In momentum representation, the Hamiltonian reads $H_0 = \sum_{\mathbf{k},\sigma} \psi_{\sigma}^{\dagger}(\mathbf{k}) \mathcal{H}_0 \psi_{\sigma}(\mathbf{k})$, where

$$\mathcal{H}_0 = \begin{pmatrix} 0 & \phi^*(\mathbf{k}) \\ \phi(\mathbf{k}) & 0 \end{pmatrix} \quad (2)$$

with $\phi(\mathbf{k}) = -t \sum_{\delta_i} e^{-i\mathbf{k}\delta_i} \equiv -\epsilon(\mathbf{k}) e^{i\varphi(\mathbf{k})}$. This Hamiltonian acts on a spinor representing the wave function on two sublattices: $\psi_{\sigma} = (\psi_{\sigma A}, \psi_{\sigma B})^T$. Accordingly, quasiparticle's excitation spectrum has two branches(bands) with the dispersion $E^{\pm}(\mathbf{k}) = \pm\epsilon(\mathbf{k})$ and⁵

$$\epsilon(\mathbf{k}) = t \sqrt{1 + 4 \cos \frac{k_x a}{2} \cos \frac{\sqrt{3} k_y a}{2} + 4 \cos^2 \frac{k_x a}{2}}. \quad (3)$$

The upper band(E^+) and the lower band(E^-) meet at six corners of the first Brillouin zone. Only two out of the six are independent, which we choose to be $\mathbf{K}_{\pm} = \pm \frac{2\pi}{a}(2/3, 0)$ as shown in Fig. 2. With an expansion around \mathbf{K}_{\pm} , one can find that the Hamiltonian (2) reduces to a massless Dirac Hamiltonian with linear dispersion $E^{\pm}(\mathbf{k}) = \pm \hbar v_F |\mathbf{k}|$. It is important to note that in monolayer graphene the pseudo-spin is defined as eigenvalue of the Pauli matrix σ_1 .

In tunneling problem, we consider the barrier of which the geometry is shown in Fig. 1. The dynamics is governed by the Schrödinger equation for an incident particle of energy E ,

$$[H_0 + V(x)]\psi = E\psi. \quad (4)$$

We solve eqn. (4) by using the standard method. At first, we assume the incident electron wave propagates along the x axis with a given energy E_i and wave vector k_i . Because V has no y dependence, the wave vector along y direction is conserved, so the wave vector along the y -direction in all the regions remains to be k_{iy} . In region I and V, the eigenstates with $\epsilon(\mathbf{k}) = E_i$ and $k_y = k_{iy}$ are fourfold degenerate as shown in Fig. 2, while the corresponding eigenfunctions are

$$\psi(\mathbf{k}_l) = \frac{1}{\sqrt{2}} \begin{pmatrix} 1 \\ \phi(\mathbf{k}_l)/E_i \end{pmatrix} e^{i\mathbf{k}_l \mathbf{r}}. \quad (5)$$

Inside the barrier, i.e, in region III, the electron's wave vectors should satisfy $\epsilon(\mathbf{q}_l) = V_0 - E_i$, $l = 1, 2, 3, 4$ and $q_{ly} = k_{iy}$. The eigenfunctions inside the barrier can be written as

$$\psi(\mathbf{q}_l) = \frac{1}{\sqrt{2}} \begin{pmatrix} 1 \\ \phi(\mathbf{q}_l)/(E_i - V_0) \end{pmatrix} e^{i\mathbf{q}_l \mathbf{r}}. \quad (6)$$

After constructing all these wave functions, the next step is to determine incident and reflected waves through the whole tunneling process which can be done with the velocities of these states

$$\begin{aligned} v_x(\mathbf{k}) &= \frac{1}{\hbar} \frac{d\epsilon(\mathbf{k})}{dk_x} \\ &= -\frac{at}{\hbar} \frac{\sin\left(\frac{k_x a}{2}\right) \left[\cos\left(\frac{\sqrt{3}k_y a}{2}\right) + 2 \cos\left(\frac{k_x a}{2}\right) \right]}{\sqrt{1 + 4 \cos\left(\frac{k_x a}{2}\right) \cos\left(\frac{\sqrt{3}k_y a}{2}\right) + 4 \cos^2\left(\frac{k_x a}{2}\right)}}. \end{aligned} \quad (7)$$

Therefore, for the right movers in Fig. 1, we require²⁰ $v_x(\mathbf{k}) > 0$; on the contrary, for the left movers, their velocity $v_x(\mathbf{k}) < 0$.

Before proceeding to the numerical calculation, it will be instructive to make some general analyses about the two different scattering processes in this system as shown in Fig. 2. In that figure, the solid arrow represents intra-valley scattering, while the dashed arrow represents inter-valley scattering. The latter one has a much larger momentum transfer ($\sim 2|\mathbf{K}_+$), hence it is usually neglected for low barrier ($V_0 \ll t$) tunneling^{7,10,20,21}. Furthermore, these two scattering processes are associated with the two operations on the pseudo-spin of the quasiparticles: intra-valley scattering flips the pseudo-spin; while during inter-valley scattering the pseudo-spin is conserved.

We can write down the general solutions in different regions^{7,10}. In region I, we have one incident wave (\mathbf{k}_1 or \mathbf{k}_3) and two reflective waves (\mathbf{k}_2 and \mathbf{k}_4), and the solutions can be expressed as

$$\Psi_{\text{I}}(\mathbf{r}) = \psi(\mathbf{k}_1) + r_1\psi(\mathbf{k}_2) + r_2\psi(\mathbf{k}_4). \quad (8)$$

Here r_1 is the intra-valley reflection amplitude and r_2 is the inter-valley reflection amplitude. In region III we have four hole states with

$$\Psi_{\text{III}}(\mathbf{r}) = f_1\psi(\mathbf{q}_1) + f_2\psi(\mathbf{q}_2) + f_3\psi(\mathbf{q}_3) + f_4\psi(\mathbf{q}_4). \quad (9)$$

Finally, in region V, we have two transmitted waves

$$\Psi_{\text{V}}(\mathbf{r}) = t_1\psi(\mathbf{k}_1) + t_2\psi(\mathbf{k}_3). \quad (10)$$

Now we need to solve the Schrödinger equation in region II and IV numerically to find the wavefunctions. Upon applying the continuity of the wave function at the boundaries, one may obtain the coefficients r , f , and t . After that one can determine the transport probability by $T = |t_1|^2 + |t_2|^2 \times v_x(\mathbf{k}_3)/v_x(\mathbf{k}_1)$. An important advantage of our model is that we can choose the incoming electron from different valleys(\mathbf{k}_1 or \mathbf{k}_3), which would lead to different tunneling properties in the results.

B. Tunneling in bilayer graphene lattice

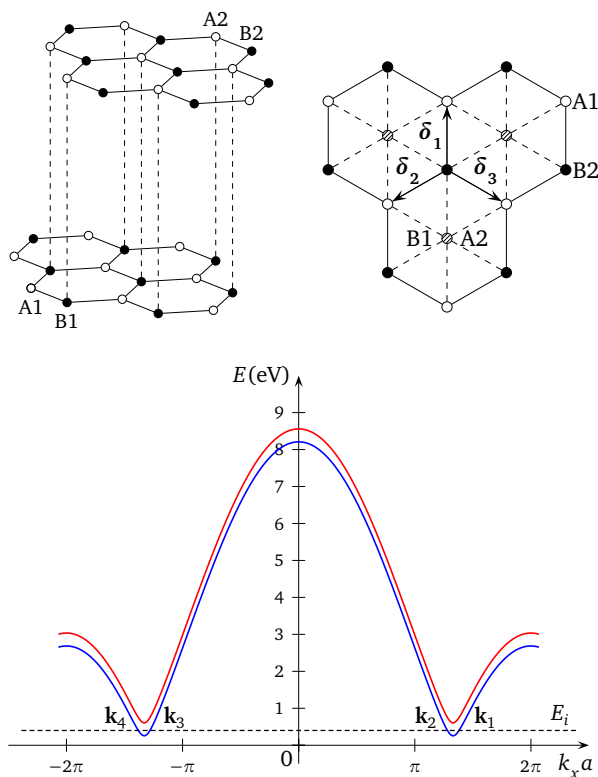


FIG. 3: Schematics of the lattice structure and the energy spectrum of bilayer graphene. Top left: Interlayer coupling t_{\perp} forms 'dimers' from pairs of A2-B1 orbitals(dashed lines), which leading to the formation of high energy bands. Top right: Top view of bilayer lattice. The only hopping mechanism between two layers is A1(open) \rightleftharpoons B2(solid) hopping via A2-B1(hash) dimer state. Bottom: Band structure of bilayer graphene. At the Dirac point, the spectrum has a gap of t_{\perp} . The pseudo-spin of lower band is +1, of upper band is -1.

Bilayer graphene consists of two monolayer stacked as in natural graphite(see Fig. 3). This so-called Bernal stacking yields a unit cell of four atoms(A1, B1, A2 and B2) resulting in four electronic bands. The tight-binding Hamiltonian

for bilayer graphene can be written as^{5,22}

$$H_0 = -t \sum_{\langle i,j \rangle, m, \sigma} \left(a_{\sigma, mi}^\dagger b_{\sigma, mj} + \text{h.c.} \right) - t_\perp \sum_{\langle 1i, 2j \rangle, \sigma} \left(a_{\sigma, 1i}^\dagger b_{\sigma, 2j} + \text{h.c.} \right), \quad (11)$$

where t_\perp ($\approx 0.35\text{eV}$) is interlayer hopping through dimer states, $m = 1, 2$ is plane index. In momentum space, the effective bilayer Hamiltonian has the form of

$$\mathcal{H}_0 = \begin{pmatrix} 0 & \phi^*(\mathbf{k}) & 0 & 0 \\ \phi(\mathbf{k}) & 0 & -t_\perp & 0 \\ 0 & -t_\perp & 0 & \phi^*(\mathbf{k}) \\ 0 & 0 & \phi(\mathbf{k}) & 0 \end{pmatrix}, \quad (12)$$

The eigenstates of Eq. (12) are four component spinors $\psi_\sigma = (\psi_{\sigma A1}, \psi_{\sigma B1}, \psi_{\sigma A2}, \psi_{\sigma B2})^T$, where $\psi_{A1, B1}$ ($\psi_{A2, B2}$) are the envelop functions associated with the probability amplitudes at the respective sublattice sites of the lower(upper) graphene sheet.

The Hamiltonian \mathcal{H}_0 determines the following spectrum of electrons in a bilayer graphene. There are four valley-degenerate bands, E_s^\pm , $s = \pm 1$, with²⁰

$$E_s^\pm(\mathbf{k}) = \pm \left| \sqrt{\frac{t_\perp^2}{4} + \epsilon^2(\mathbf{k})} + s \frac{t_\perp}{2} \right|, \quad (13)$$

where $\epsilon(\mathbf{k})$ is the dispersion of a monolayer graphene. The dispersion E_{-1}^\pm describe low energy bands while E_{+1}^\pm describe higher energy bands as shown in Fig. 3. One can see that low energy excitations exhibit parabolic dispersion, while for larger k values, the linear $E - k$ behavior is recovered.

An important difference in the eigenfunctions between the monolayer and the bilayer graphene is that in the latter case there are eight eigenstates (two bands) for a given energy E_i and fixed k_y . Accordingly, for four component spinor ψ_σ , the pseudo-spin in bilayer graphene is defined as eigenvalue of Dirac matrix

$$\gamma_1 = \begin{pmatrix} 0 & 0 & 0 & 1 \\ 0 & 0 & 1 & 0 \\ 0 & 1 & 0 & 0 \\ 1 & 0 & 0 & 0 \end{pmatrix}. \quad (14)$$

As a result, the pseudo-spin of state E_s^\pm in bilayer graphene is $\mp s$. So the lower band (E_{-1}^\pm) in Fig. 3 is associated with pseudo-spin $+1$, and the upper band (E_{+1}^\pm) with -1 . Therefore, both inter- and intra-valley scattering do not flip the pseudo-spin. This feature is totally different from monolayer structure. Moreover, in our computation, the energy of incident wave satisfies $E_i \ll t_\perp$ as this will likely be the experimental situation. So in region I and V we have four of these states ($\mathbf{k}_{1,2,3,4}$) correspond to propagating waves (E_{-1}^\pm) and the other four ($\mathbf{k}_{1,2,3,4}$) to evanescent ones (E_{+1}^\pm). These evanescent modes have a complex value of the momentum in the x -direction and must be considered to fulfill the boundary conditions. It is worth noting that the incident electron in bilayer lattice could only reside on band E_{-1}^\pm with pseudo-spin $+1$.

By solving Hamiltonian in Eq. (12), one finds the eigenvectors (V is external potential),

$$\psi_s^\pm(\mathbf{k}) = C \begin{pmatrix} \alpha(\mathbf{k}) \phi^*(\mathbf{k}) / (E_s^\pm - V) \\ \alpha(\mathbf{k}) \\ (E_s^\pm - V) / \phi(\mathbf{k}) \\ 1 \end{pmatrix} e^{i\mathbf{k}\cdot\mathbf{r}}, \quad (15)$$

where C is normalization constant, and $\alpha(\mathbf{k})$ is defined as

$$\alpha(\mathbf{k}) = - \left[(E_s^\pm - V)^2 - |\phi(\mathbf{k})|^2 \right] / t_\perp \phi(\mathbf{k}). \quad (16)$$

Note again that for propagating waves, k_x is real; while for evanescent solutions, k_x is complex.

Similar to the case of the monolayer graphene, by calculating the group velocity $v_x(\mathbf{k}) = d\epsilon(\mathbf{k}) / \hbar dk_x$, we can prove that $\mathbf{k}_{1,3}$ are right movers (transmission waves) while $\mathbf{k}_{2,4}$ are left movers (reflective waves). On the other hand, to

select appropriate evanescent states, since κ_{lx} ($l = 1, 2, 3, 4$) are complex numbers, we should consider the asymptotic behavior of these states at $\pm\infty$.

Finally, the general solutions for bilayer graphene can be expressed as¹⁰(incident electron coming from \mathbf{k}_1)

$$\Psi_{\text{I}}(\mathbf{r}) = \psi_{-1}^+(\mathbf{k}_1) + r_1\psi_{-1}^+(\mathbf{k}_2) + r_2\psi_{-1}^+(\mathbf{k}_4) + r_3\psi_{+1}^+(\boldsymbol{\kappa}_2) + r_4\psi_{+1}^+(\boldsymbol{\kappa}_4), \quad (17a)$$

$$\Psi_{\text{III}}(\mathbf{r}) = \sum_{l=1}^4 [f_l\psi_{-1}^-(\mathbf{q}_l) + g_l\psi_{+1}^-(\boldsymbol{\tau}_l)], \quad (17b)$$

$$\Psi_{\text{V}}(\mathbf{r}) = t_1\psi_{-1}^+(\mathbf{k}_1) + t_2\psi_{-1}^+(\mathbf{k}_3) + t_3\psi_{+1}^+(\boldsymbol{\kappa}_1) + t_4\psi_{+1}^+(\boldsymbol{\kappa}_3). \quad (17c)$$

Here \mathbf{q}_l and $\boldsymbol{\tau}_l$ are the corresponding wavevectors for propagating states (E_{-1}^-) and evanescent states (E_{+1}^-) inside the barrier. Then by solving Eq. (4) numerically in II and IV, and utilizing continuity of the wave functions on four sublattices at boundaries, one may obtain the transmission coefficients for a bilayer graphene lattice by using the same equations as in the case of monolayer structure.

III. NUMERICAL RESULTS AND DISCUSSION

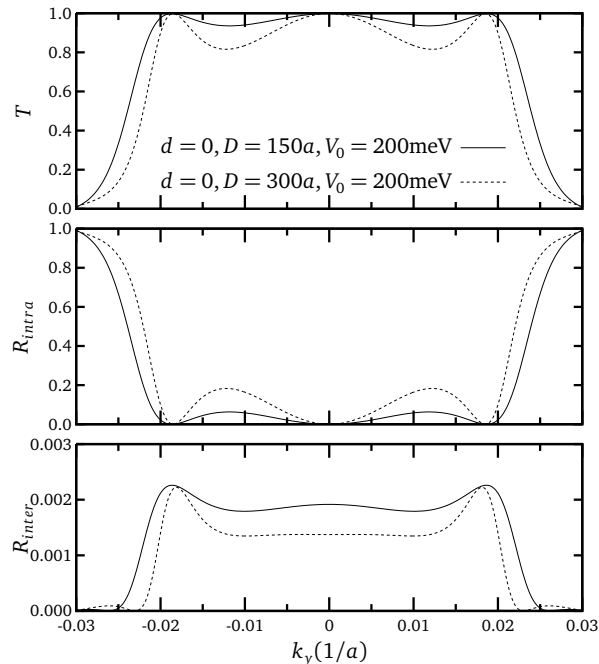


FIG. 4: k_y dependence of transmission coefficients in monolayer graphene for abrupt potential barrier ($d = 0$). The incident electron comes from valley \mathbf{K}_+ with energy 80meV. The potential height is 200meV with different widths $D = 150a$ or $300a$. During the whole tunneling process, we always have $T + R_{intra} + R_{inter} = 1$ to ensure current conservation. Note that different scaling are used in R_{intra} and R_{inter}

We first calculate the transmission probabilities of charge carriers through monolayer graphene lattice. The results are depicted in Figs. 4 and 5. Fig. 4 shows examples of k_y dependence of transmission probability for an abrupt potential barrier with height $V_0 = 200\text{meV}$. Under this potential barrier, incident electron continues propagating as a hole in region III. The solid lines and dashed lines correspond to the potential width $D = 150a$ and $300a$, respectively. It is seen from the figure that, averagely speaking, the intra-valley scattering coefficient is much larger than inter-valley scattering coefficient. This is because in scattering process (see Fig. 2), the intra-valley momentum transfer is much smaller than the inter-valley momentum transfer ($\sim 2|\mathbf{K}_+|$), thus should have larger possibilities. It is also clear from the figure that the barrier remains nearly perfectly transparent^{7,10} ($T \sim 1$) for small k_y . This phenomenon is unique to relativistic quasiparticles that incident electrons can be scattered into hole states inside the barrier. In this figure,

the incident particle is in state \mathbf{k}_1 which comes from valley \mathbf{K}_+ . We can also choose the incident particle coming from valley \mathbf{k}_3 . The difference of these two results is very small, which means that valley discrepancy is very tiny in low-energy case.

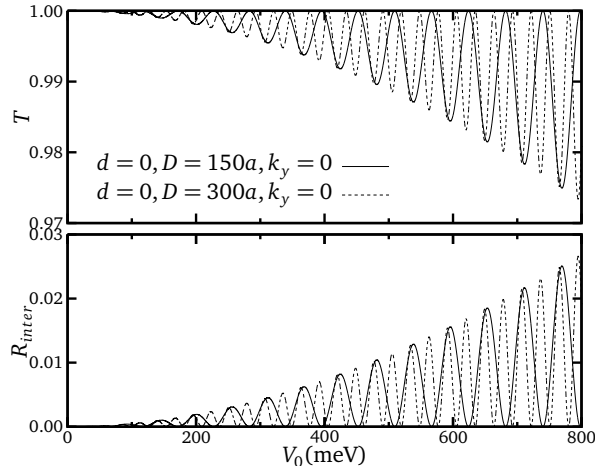


FIG. 5: Transmission probability T and inter-valley scattering amplitude R_{inter} for normally incident electrons through monolayer graphene as a function of external potential height. The incident electron comes from valley \mathbf{K}_+ with energy 80meV. The width of the barrier is $d = 0$ and $D = 150a$ or $300a$. For normal incident tunneling, we always have $R_{intra} \equiv 0$.

Now let's examine the normally incident cases, i.e., $k_y = 0$. The transmission coefficients are plotted in Fig. 5, where we find that intra-valley scattering is totally suppressed. This can be understood in terms of the conservation of pseudo-spin. In normal incident tunneling, pseudo-spin becomes a good quantum number through the whole process. Therefore, spin flipping is not allowed when quasiparticles propagating in this system. Hence, inter-valley scattering is the only reflection mechanism. However, since momentum transfer $\mathbf{k}_1 \rightarrow \mathbf{k}_4$ is quite large, R_{inter} is very small (~ 0.01). So if we neglect the inter-valley scattering probability²¹, then monolayer graphene can be regarded as a condensed matter version Klein paradox^{7,10}. Furthermore, we can see that the transmission amplitude shows a resonant feature that the envelope of T decreases monotonically as V_0 increases. This can be understood as Dirac-like particle's resonance tunneling, where the resonance frequency and magnitudes varies significantly with different barrier widths. With increasing D , the resonance frequency increases obviously as shown in Fig. 5, while the envelope of transmission amplitude remains the same. On the other hand, the magnitude of oscillation also depends sensitively on barrier width d . By increasing d , inter-valley scattering amplitude falls noticeably. For example, in case of $d = 3a$, the inter-valley scattering amplitude falls to the order of 10^{-5} when $V_0 = 800\text{meV}$. Thus one can achieve nearly perfect transmission even with very high barrier height by smoothing the potential step.

By now we have investigated low-barrier ($V_0 \ll t$) tunneling in monolayer graphene by choosing incident particle as \mathbf{k}_1 which comes from \mathbf{K}_+ . If the incident electron comes from valley \mathbf{K}_- , our result shows no obvious difference with valley \mathbf{K}_+ . To amplify this valley-contrasting feature, we have to look at the high-barrier ($V_0 \sim t \approx 2.8\text{eV}$) limit of the tunneling problem. The results of normally incident transmission are depicted in Fig. 6.

In this figure, one can see that the situation is completely different from low-barrier scattering. Besides the resonant feature in the transmission pattern, incident electrons coming from \mathbf{K}_+ and \mathbf{K}_- have totally distinct tunneling properties. The origin of this valley dissimilarity is due to the unique energy dispersion in graphene as shown in Fig. 2. At first, it is worth noting that pseudo-spin is a good quantum number in normally incident tunneling and the incident electrons might have two types of pseudo-spin, $+1(\mathbf{K}_+)$ or $-1(\mathbf{K}_-)$. For low potential barrier, i.e. $V_0 < E_i + t$, there are four propagating states in region III. Two of these states have pseudo-spin $+1$, while the other two have pseudo-spin -1 . Therefore, no matter which incident state we select, the pseudo-spin inside the barrier can always match the incoming quasiparticle. So in low-barrier limit, resonant pattern is found in the transmission amplitude of both valleys.

On the other hand, for high potential barrier, i.e. $V_0 > E_i + t$, two propagating states with pseudo-spin -1 in region III turn to evanescent states²³, while the propagating states with pseudo-spin $+1$ remain the same. As a result, different incident electrons come from different Dirac points \mathbf{K}_+ and \mathbf{K}_- must have distinct transmission properties. For incident electron in state \mathbf{k}_1 with pseudo-spin $+1$, the potential barrier is always transparent. On the contrary, for electron coming from state \mathbf{k}_3 with pseudo-spin -1 , it cannot penetrate the potential barrier if $V_0 > E_i + t$. Moreover, it is also shown in Fig. 6 that the possibility of inter-valley scattering can be notably enhanced if we increase the potential height V_0 . Using these tunneling properties, one may obtain valley polarized electron

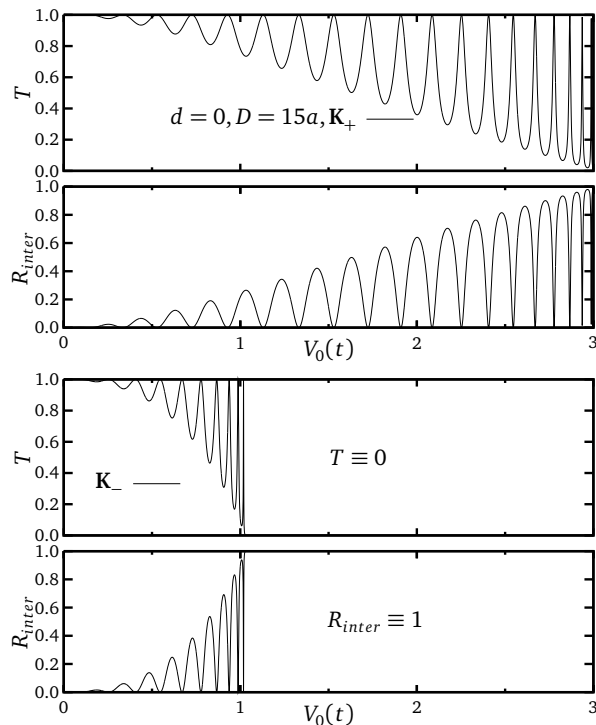


FIG. 6: Transmission probability T and inter-valley scattering amplitude R_{inter} for normally incident electrons through monolayer graphene as a function of external potential height. The incident electron is of energy 80meV and may have valley polarization of Dirac points \mathbf{K}_+ or \mathbf{K}_- . The potential width is $d = 0$ and $D = 15a$. Top: Incident electron comes from \mathbf{K}_+ . Bottom: Incident electron comes from \mathbf{K}_- .

currents^{14,17} in monolayer graphene by adding appropriate external gate voltage.

Similar to low-barrier limit, we find that the magnitude of inter-valley scattering amplitude also depends very sensitively on potential height V_0 and the thickness of region II, IV in Fig. 1. If we smooth the potential step by increasing d , then the envelope of inter-valley scattering coefficient shrinks much smaller very quickly. Furthermore, although inter-valley scattering requires a very large momentum transfer, we can still achieve very high scattering probability by increasing the barrier height. Our result shows that charge carriers in monolayer graphene, when subjected to a high potential barrier, exhibit totally distinct tunneling features from Dirac fermions.

For the case of bilayer graphene, the computational results are shown in the following figures. Some representatives k_y dependence are depicted in Fig. 7, and these should be contrasted to the case of monolayer in Fig. 4. The result is totally different since the bilayer energy spectrum (see Fig. 3) splits into two bands. One can see that for potential barrier (V_0) higher than the energy of incident quasiparticle (E_i), it remains nearly totally reflective for small k_y . In normally incident ($k_y = 0$) case, it becomes totally reflective even though there are plenty of electronic states inside the barrier^{7,20}. This behavior, which is similar to the tunneling property of non-chiral massive quasiparticles, is in obvious contrast to monolayer graphene, where massless Dirac fermions are always perfectly transmitted for small k_y ¹⁰.

To understand this feature, let's take a look at the result of normally incident case as shown in Fig. 8. One can see in this figure that the transmission probability $T \sim 0$ if

$$E_i < V_0 < E_i + t_{\perp}, \quad (18)$$

and the transmission amplitudes exhibit nonresonant feature within this range. This result is valley independent and can be explained in terms of pseudo-spin conservation in normal incident tunneling. As one can see in Fig. 3, under the condition of Eq. (18), all the propagating states in region III are hole states E_{-1}^- with pseudo-spin -1 . While the incoming wave, no matter which valley it comes from, must have pseudo-spin $+1$. As a result, the only survival tunneling mechanism is via evanescent hole states E_{+1}^- . Therefore, $(E_i, E_i + t_{\perp})$ becomes a non-penetrative region for bilayer graphene. This conclusion is coincide with the k_y dependence as we depicted in Fig. 7.

On the other hand, beyond this non-penetrative range, the resonant feature is found again for all barrier heights as the pseudo-spin of propagating states in region III can always match the incoming electron. Further more, valley difference is not obvious in low energy limit when $V \ll t$, which is the same as the case in monolayer graphene

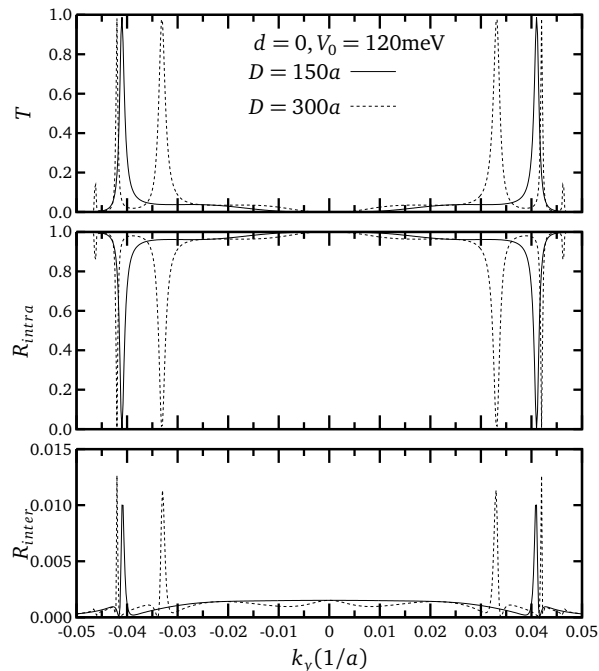


FIG. 7: k_y dependence of transmission coefficients in bilayer graphene for abrupt potential barrier ($d = 0$). The incident electron comes from valley \mathbf{K}_+ with energy 80meV. The potential height is 120meV with different widths $D = 150a$ or $300a$.

under low-barrier limit. While for high barrier tunneling, the transmission patterns of different Dirac points are notably distinct. This distinction is due to the inter-valley momentum transfer $|\mathbf{k}_1 - \mathbf{k}_4| = 2|\mathbf{k}_1|$ is larger than $|\mathbf{k}_3 - \mathbf{k}_2| = 2|\mathbf{k}_3|$. So intrinsically the probability of inter-valley scattering amplitudes $\mathbf{k}_1 \rightarrow \mathbf{k}_4$ should be smaller than $\mathbf{k}_3 \rightarrow \mathbf{k}_2$. In Fig. 8, this difference is amplified by high potential barrier and shows the existence of valley polarized current in bilayer graphene¹⁷. Moreover, in Fig. 8, the patterns of reflection coefficient R_{intra} are almost the same. This can be understood as intra-valley momentum transfer in two valleys are equal to each other

$$|\mathbf{k}_1 - \mathbf{k}_2| = |\mathbf{k}_3 - \mathbf{k}_4|. \quad (19)$$

Finally, we also point out that the dependence of transmission amplitude on d and D in bilayer graphene is the same as the result in monolayer structure. If we increase the width of region III, the envelope of T curve does not change while the period of resonant oscillation decreases. On the other hand, if we smooth the potential step by broadening the width of region II and IV, the amplitude of inter-valley scattering falls very quickly to smaller than 10^{-5} . However, intra-valley scattering probability does not depend on d in our computation. Thus we can tune the proportion of these two scattering mechanisms separately by adding arbitrary electronic fields at the edges of the external potential barrier.

Before closing, just a comment on our calculation. Actually, previous studies of tunneling properties in monolayer (bilayer) graphene that were based on a continuum model have used a massless Dirac fermion (massive excitations) approximation, which is expected to be accurate for low-energy quasiparticles^{5,6,7,10,20,22}. Hence, inter-valley scattering is rarely considered in investigating the transport properties of graphene systems²⁴ because of the large separation of Dirac points in momentum space. Moreover, valley contrasting physics is also absent in low-energy quasiparticle's tunneling features in this system. However, our result shows that, although low-energy tunneling in monolayer (bilayer) graphene is sufficiently described by massless (massive) fermion approximation, in high-energy limit there will be a significant deviation between this approximation and the real system¹⁸. With the increasing of barrier height, inter-valley scattering can be realized and amplified significantly as shown in Figs. 6 and 8. At the same time, we find that valley discrepancy in the tunneling problem would be gradually magnified by strengthening the external potential. These effects, which are distinct from the properties of low-energy limit, lead to the possibility of generating, detecting and controlling valley polarized currents in graphene systems by electric means^{14,17}.

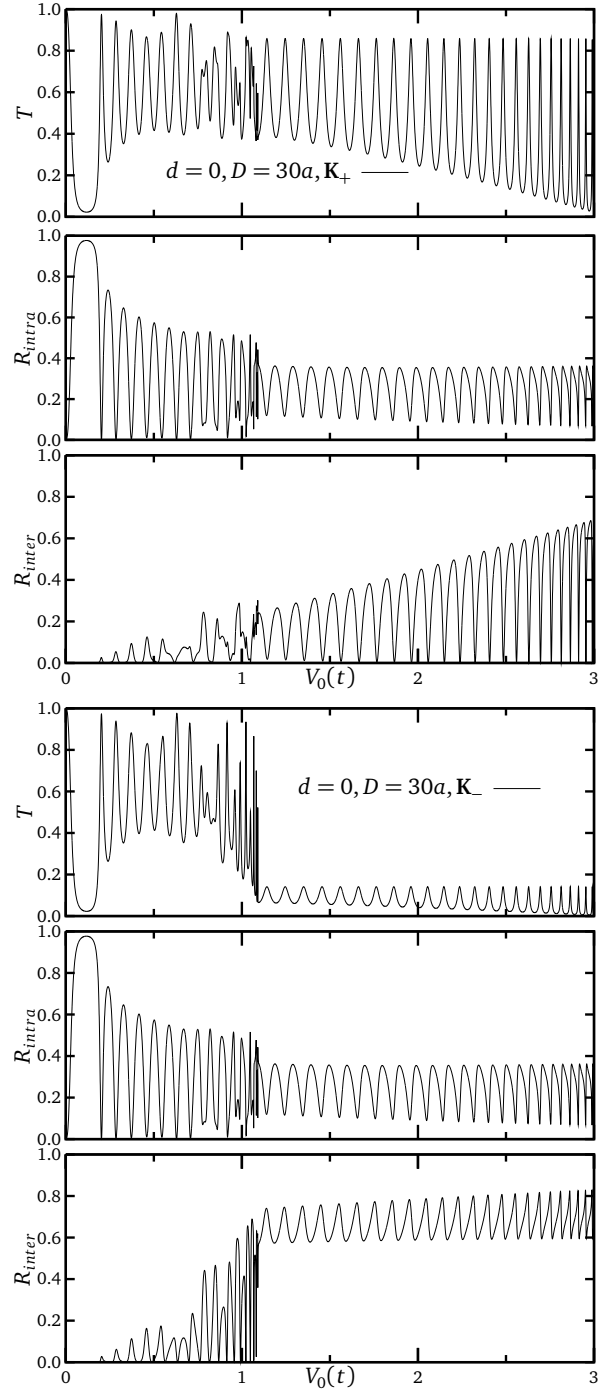


FIG. 8: Transmission coefficients for normally incident waves through bilayer graphene as a function of external potential height. The incident electron is of energy 80meV and may have valley polarization of Dirac points \mathbf{K}_+ or \mathbf{K}_- . Potential width is $d = 0$ and $D = 30a$. Top: Incident electron comes from \mathbf{K}_+ . Bottom: Incident electron comes from \mathbf{K}_- .

IV. SUMMARY AND CONCLUSION

Based on a tight-binding model, we have investigated single particle tunneling properties through potential barrier in monolayer and bilayer graphene lattices. The normal incidence and angular dependent transmission probabilities for two kinds of graphene structure have been numerically calculated. Our result illustrates that the tunneling behavior in graphene is much richer than what was anticipated in massless Dirac fermion approximation. Furthermore, it is shown that both of the intra- and inter-valley scattering probability are strongly dependent on the applied external

potential, forming the basis for the valley-based electronics applications of these systems. Our results may provide an important reference to the design of electron devices based on graphene materials.

-
- ¹ K. S. Novoselov, A. K. Geim, S. V. Morozov, D. Jiang, Y. Zhang, S. V. Dubonos, I. V. Grigorieva, and A. A. Firsov, *Science* **306**, 666 (2004).
- ² P. R. Wallace, *Phys. Rev.* **71**, 622 (1947).
- ³ Vitor M. Pereira, J. M. B. Lopes dos Santos, and A. H. Castro Neto, *Phys. Rev. B* **77**, 115109 (2008).
- ⁴ A. K. Geim, and K. S. Novoselov, *Nature Mat.* **6**, 183 (2007).
- ⁵ A. H. Castro Neto, F. Guinea, N. M. R. Peres, K. S. Novoselov, and A. K. Geim, arXiv:0709.1163v2.
- ⁶ K. S. Novoselov, A. K. Geim, S. V. Morozov, D. Jiang, M. I. Katsnelson, I. V. Grigorieva, S. V. Dubonos, and A. A. Firsov, *Nature* **438**, 197 (2005).
- ⁷ M. I. Katsnelson, K. S. Novoselov, A. K. Geim, *Nature Phys.* **2**, 620 (2006).
- ⁸ J. M. Pereira, Jr., V. Mlinar, F. M. Peeters, and P. Vasilopoulos, *Phys. Rev. B* **74**, 045424 (2006).
- ⁹ V. V. Cheianov, and V. I. Fal'ko, *Phys. Rev. B* **74**, 041403(R) (2006).
- ¹⁰ Chunxu Bai and Xiangdong Zhang, *Phys. Rev. B* **76**, 075430 (2007).
- ¹¹ N. Stander, B. Huard, and D. Goldhaber-Gordon, arXiv:08062319v1.
- ¹² O. Klein, *Z. Phys.* **53**, 157 (1929).
- ¹³ T. Ando, and T. Nakanishi, *J. Phys. Soc. Jpn.* **67**, 1704 (1998).
- ¹⁴ Di Xiao, Wang Yao, and Qian Niu, *Phys. Rev. Lett.* **99**, 236809 (2007).
- ¹⁵ C. L. Kane, and E. J. Mele, *Phys. Rev. Lett.* **95**, 226801 (2005).
- ¹⁶ S. Cho, Y.-F. Chen, and M. S. Fuhrer, *Appl. Phys. Lett.* **91**, 123105 (2007).
- ¹⁷ A. Rycerz, J. Tworzydło, and C. W. J. Beenakker, *Nature Phys.* **3**, 172 (2007).
- ¹⁸ P. Plochocka, C. Faugeras, M. Orlita, M. L. Sadowski, G. Martinez, M. Potemski, M. O. Goerbig, J. N. Fuchs, C. Berger, and W. A. de Heer, *Phys. Rev. Lett.* **100**, 087401 (2008).
- ¹⁹ Eduardo V. Castro, K. S. Novoselov, S. V. Morozov, N. M. R. Peres, J. M. B. Lopes dos Santos, Johan Nilsson, F. Guinea, A. K. Geim, and A. H. Castro Neto, *Phys. Rev. Lett.* **99**, 216802 (2007).
- ²⁰ Johan Nilsson, A. H. Castro Neto, F. Guinea, and N. M. R. Peres, *Phys. Rev. B* **76**, 165416 (2007).
- ²¹ Cheol-Hwan Park, Li Yang, Young-Woo Son, Marvin L. Cohen, and Steven G. Louie, *Nature Phys.* **4**, 213 (2008).
- ²² Edward McCann and Vladimir I. Fal'ko, *Phys. Rev. Lett.* **96**, 086805 (2006).
- ²³ R. Danneau, F. Wu, M. F. Craciun, S. Russo, M. Y. Tomi, J. Salmilehto, A. F. Morpurgo, and P. J. Hakonen, *Phys. Rev. Lett.* **100**, 196802 (2008).
- ²⁴ S. V. Morpurgo, and F. Guinea, *Phys. Rev. Lett.* **97**, 196804 (2006).